chemosensors

MDPI

Article

Multiplexed Detection of Human Papillomavirus Based on AzaBODIPY-Doped Silica-Coated Polystyrene Microparticles

Gugu Kubheka [1], Estela Climent [2], Charlie Tobias [2], Knut Rurack [2,*], John Mack [1,*] and Tebello Nyokong [1]

[1] Institute for Nanotechnology Innovation, Rhodes University, Makhanda 6140, South Africa
[2] Chemical and Optical Sensing Division, Bundesanstalt für Materialforschung und -prüfung (BAM), Richard Willstätter Str. 11, 12489 Berlin, Germany
* Correspondence: knut.rurack@bam.de (K.R.); j.mack@ru.ac.za (J.M.)

Abstract: Human papillomavirus (HPV) DNA detection can enable the early diagnosis of high-risk HPV types responsible for cervical cancer. HPV detection is also essential for investigating the clinical behavior and epidemiology of particular HPV types, characterization of study populations in HPV vaccination trials and monitoring the efficacy of HPV vaccines. In this study, two azaBODIPY dyes (**1** and **2**) were used as references and were doped into polystyrene particles (**PS40**), while a short HPV DNA single strand was used as a target molecule and was covalently bound to the silica shell. These particles were employed as optical probes in 1:1 hybridization assays, and their potential applicability as a tool for multiplex assays for the detection of different strands of HPV was evaluated using flow cytometry. A good separation in the fluorescence of the four different concentrations prepared for each dye was observed. To perform the hybridization assays, HPV18, HPV16, HPV11 and HPV6 single strands were attached to the particles through EDC-mediated coupling. The **c-DNA-1-PS40** and **c-DNA-2-PS40** particles exhibited low limit of detection (LOD) and quantification (LOQ) values for HPV11, and a narrow detection range was obtained. Multiplexed assay experiments were successfully performed for both particles, and the results proved that **c-DNA-1-PS40** could potentially be used as a tool for multiplexing assays and merits further in-depth study in this context.

Keywords: azaBODIPY; flow cytometry; multiplex assay; single assay; polystyrene microparticles; silica shell; human papillomavirus

Citation: Kubheka, G.; Climent, E.; Tobias, C.; Rurack, K.; Mack, J.; Nyokong, T. Multiplexed Detection of Human Papillomavirus Based on AzaBODIPY-Doped Silica-Coated Polystyrene Microparticles. *Chemosensors* **2023**, *11*, 1. https://doi.org/10.3390/chemosensors11010001

Academic Editor: Run Zhang

Received: 31 October 2022
Revised: 7 December 2022
Accepted: 8 December 2022
Published: 20 December 2022

1. Introduction

The fluorescence of organic dyes has been extensively used as a signal transduction tool to provide highly sensitive fluorescence-based detection techniques [1,2]. However, some of these organic fluorophores have major drawbacks, such as environmental sensitivity due to their molecular nature, photostability and their bioconjugation possibilities [3]. The absence of functional groups for further conjugation to biomolecules without interfering with the target's binding specificity or causing it to precipitate can be problematic [3,4]. To combat these limitations, polystyrene or silica particles can be used as carrier platforms for the analysis since they can be produced at low cost, in large batches and different sizes, and because they can be facilely doped with organic dyes [5–8]. While silica nanoparticles are mainly used for ensemble measurements, polystyrene (PS) microparticles are commonly used in single particle-based methods, including many commercial assays, because of their high refractive index and excellent scattering properties [9,10]. However, combining polystyrene and silica particles results in beads that combine the properties of easy modification and tolerance to organic (co-)solvents with the presence of organic functional groups, a low sedimentation tendency and good scattering properties [11,12]. AzaBODIPY-doped PS particles coated with a silica shell were used for the assays in this study. Similar BODIPY-doped particles have been studied previously [13,14]. The dyes

are used as a reference and are doped into polystyrene particles [14], while short DNA single-strands corresponding to specific genetic sequences of the Human Papillomavirus (HPV) were used as a target, the complementary strands of which were covalently bound to the silica shell. The detection of HPV is essential due to its relevance as a carcinogen and its presence in many different diseases, including cervical cancer, the second most common cancer among women worldwide [15]. Hence, HPV DNA detection can enable the early diagnosis of high-risk HPV types responsible for cervical cancer.

In an earlier work, some of us reported polystyrene (PS) microparticles with convergently grown mesoporous silica shells as a promising tool for multiplexed bioanalytical assays [14]. In that study, two different PS particles were used, i.e., particles prepared with poly(vinylpyrrolidone) of molecular weights 10 and 40 kDa as stabilizing agents, PVP10 and PVP40, yielding PS10 and PS40, in combination with mesoporous silica particles to detect HPV types using a BODIPY dye as a reference. In this study, two unfunctionalized azaBODIPY dyes were separately doped into PS40 particles in combination with a non-porous silica shell for the multiplex detection of HPV DNA sequences by flow cytometry. AzaBODIPY dyes have potential in this regard due to their structural versatility, photochemical stability, high molar absorption coefficients and tunable emission wavelengths [16].

Microparticles encoded with combinations of fluorophores of different fluorescence wavelengths at different intensity levels have proved useful for the multiplexed detection of biomarkers through their laser excitation and flow cytometry detection setups [4,10,17]. Multiplex analyses can simultaneously perform multiple discrete assays in a single tube with the same sample [18]. In comparison to large-scale traditional assays such as ELISAs and microarrays, which require analysis of one antigen at a time and relatively large volumes of sample for multiple assays, bead-based suspension array technology (SAT) is an attractive alternative [18–21]. SAT based on spherical microparticles is a low-cost, flexible and high-throughput method capable of simultaneous detection of multiple molecular targets in a single sample (multiplexed analysis) using small volumes of the sample. In this method, for a successful multiplexed analysis, each bead must be encoded with a unique identifier to facilitate the quantification of the attached probe molecule [18–21].

The doping of identically-sized particles with two different dyes, emitting at two different wavelengths, can be used to achieve this type of assay [22]. This method circumvents problems such as particle aggregation, which compromises size-coded bead assays, while allowing for higher-number multiplexing. The aim of this study is to use PS particles doped with azaBODIPY dyes, coated with a silica shell and appropriately functionalized to analyze their sensitivity, general functionality and utility for use in flow-cytometry for DNA hybridization assays. Specific genetic sequences of different types of human papillomavirus (HPV) were chosen as the analytes for both single and multiplexed assays. The multiplexed assays were studied on four HPV types, 6, 11, 16 and 18.

2. Materials and Methods

2.1. Materials

Absolute ethanol (EtOH), tetraethylorthosilicate (TEOS), ammonia, 3-aminopropyltriethoxysilane (APTES), methanol (MeOH), hydrochloric acid (HCl) (37%), pentylamine, succinic anhydride, N,N-dimethylformamide (DMF), amino-modified DNA, complementary (c-DNA), target sequence DNA (t-DNA), 2-(N-morpholino)ethanesulfonic acid (MES), 1-(3-dimethylaminopropyl)-3-ethylcarbodiimide (EDC), N-hydroxysuccinimide (NHS) solution, magnesium chloride ($MgCl_2$), tetramethylammonium chloride (TMAC), ethylenediaminetetraacetic acid (EDTA), trisaminomethane (Tris), sodium dodecyl sulfate (SDS) and tetrahydrofuran (THF) were purchased from Sigma-Aldrich. AzaBODIPYs **1** and **2** were synthesized according to the reported literature procedures except for the modifications noted for **1** (Figure S1 in Supplementary Information) below [23–28]. The photophysical properties [28,29] are provided in Figure S2 and Table S1 in Supplementary Information. The anionic PS40 polystyrene core (**PS40**) was synthesized as reported earlier [11]. Limits of detection (LOD, according to DIN 32645:2008-11) and limits of quantification (LOQ) were determined according to

the procedures reported in [14,30]; for more experimental details, see the Supplementary Information.

2.2. Equipment

^{1}H NMR spectra were recorded at room temperature in $CDCl_3$ on a Bruker AMX 600 instrument operating at 600 MHz. Transmission electron microscopy (TEM) images were obtained using a JEOL TEM 1210 transmission electron microscope at a 100 kV accelerating voltage. TEM samples were prepared by placing a drop of conjugate or nanoparticle solution on the sample grid and allowing it to dry prior to measurements. Ultraviolet-visible (UV–vis) absorption spectra were measured for solution studies at room temperature on a Shimadzu UV-2550 and an Analytik Jena Specord 210 plus spectrophotometer with a 1 cm pathlength quartz cuvette. Energy dispersive (EDX) spectroscopy was carried out on an INCA PENTA FET coupled to the VAGA TESCAM using 20 kV accelerating voltage. Thermogravimetric analysis (TGA) was performed using a Perkin Elmer TGA 4000 analyzer. The analysis was carried out under a nitrogen flow rate of 120 cm^{-3} min^{-1}. The weighed sample masses were heated from 50 to 850 °C at a heating rate of 10 °C min^{-1}. Flow cytometric analysis was performed on a BD Accuri C6 equipped with a 488 and 635 nm argon and diode laser for excitation, respectively. Forward-scattered (FSC) and sideward-scattered light (SSC) were detected at 180 and 90°, respectively, with 488 nm bandpass filters and gains of 137 and 180. Fluorescence (FL1) was detected at 90° with a 520−50 band-pass filter and a gain of 650. The fluorescence in channels FL3 and FL4 (red channel, 675/25 nm; λ_{ex} = 650 nm) were used for recording the analytical signals and for decoding in the multiplexing experiments. All samples were measured in dispersion using water at a concentration of $\approx 1 \times 10^{-5}$ % (w/v). Each run was performed under the same instrumental settings with a run time of 60 s for all the experiments. Results are reported by gating the signal appropriately, followed by data export to Origin 9.1 (OriginLab) for further data handling.

2.3. Synthesis of AzaBODIPY 1

A modified synthetic procedure was used to synthesize azadipyrromethane **1a** (Scheme 1). A mixture of a 1,3-(*bis*-(hetero)aryl)-4-nitrobutanone **a** (1 mmol) and urea (35 mmol) was refluxed in 50 mL of *n*-BuOH: AcOH (4:1) for 24 h. The dark blue product precipitated from the solution. The dark brown reaction mixture was filtered, and the product was recrystallized from dichloromethane/hexane (1:4) to give pure product **1a** as a dark blue solid.

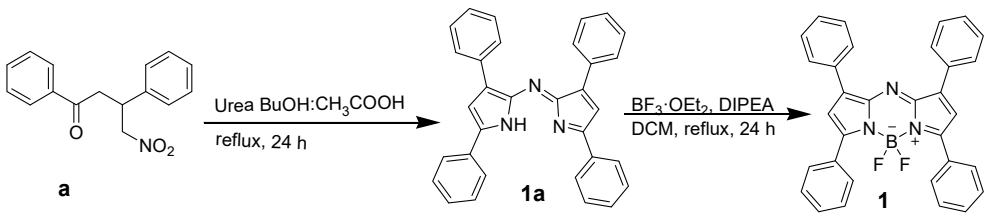

Scheme 1. Synthesis of azadipyrromethene **1a** and azaBODIPY **1**.

Azadipyrromethene **1a** obtained in 98% yield; ^{1}H NMR (600 MHz, $CDCl_3$): δ/ppm 7.33−7.36 (2H, m, Ar-H), 7.44−7.55 (12H, m, Ar-H), 7.76 (2H, d, J = 7.1 Hz, Ar-H), 7.90 (2H, s, Ar-H) and 8.22 (4H, d, J = 7.1 Hz, Ar-H).

Diisopropylamine (0.8 mL, 4.8 mmol) was added to a solution of **1a** (1 mmol) in dichloromethane (50 mL), and the mixture was stirred for 1 h. $BF_3{\cdot}OEt_2$ (0.6 mL, 5.0 mmol) was added at room temperature, and the resulting mixture was refluxed until the starting material was completely converted (ca. 2 h) to the corresponding product (monitored with thin layer chromatography). The cold reaction mixture was diluted with water and extracted twice with dichloromethane (100 mL). The combined organic layers were dried with sodium sulfate and concentrated in vacuo. The crude products were purified by flash

chromatography using dichloromethane/hexane (2:1) as eluent to obtain the products as shiny coppery-colored crystals.

AzaBODIPY 1 obtained in 62% yield; IR (νmax/cm^{-1}): 2953 (=C-H stretch), 2916−2849 (-C-H stretch), 1682 (C=N stretch), 1544–1504 (Ar C-C), 1340–1027 (C-N stretch); ^{1}H NMR (600 MHz, $CDCl_3$): δ/ppm 7.47 (2H, s, Ar-H), 7.50 (2H, t, J = 7.2 Hz, Ar-H), 7.53–7.56 (10H, m, Ar-H), 8.15–8.17 (4H, m, Ar-H) and 8.25 (4H, d, J = 9.0 Hz, Ar-H).

*2.4. Preparation of **PS40** Particles*

Polyvinylpyrrolidone (PVP)-stabilized microparticles were synthesized by dispersion polymerization with 4,4-azobis(4-cyanovaleric acid) (ACVA) as the initiator. First, 1.7 g (1.8 weight % (*w*/*w*) with regard to total weight of solvent) of the stabilizer (PVP40) was dissolved in 100 mL ethanol in a 250 mL 3-necked round-bottom flask with a magnetic stirrer. The solution was heated to 75 °C in an oil bath. ACVA was weighed separately (2.1 weight % (*w*/*v*) with regard to the volume of monomer) and dissolved in 20 mL ethanol. Styrene (9.6% (*w*/*w*) with regard to the total weight of solvent) was filtered through a basic alumina column to remove the stabilizer and then added to the ACVA solution. Both solutions were degassed simultaneously with an Ar stream for 30 min. Afterwards, the solution containing ACVA and styrene was directly transferred to the preheated PVP solution and the mixture was stirred for 24 h at 500 rpm. The particles were subsequently separated from the solution by centrifugation and washed thrice with methanol. The microparticles were obtained as a white solid after drying overnight in a vacuum oven. The product was stored at room temperature without any further treatment.

*2.5. Doping of **PS40** Particles*

A stock solution (5%) was prepared with 250 mg of **PS40** in 5 mL of Milli-Q water. 1.3 mL of this solution was added to 130 µL of THF and immediately put on a rotator at 40 rpm at room temperature. Then, 300 µL of ca. 5% anionic polystyrene suspension and 30 µL of a solution of dye **D** (**D** = **1** or **2**) in THF were added, and the mixture was immediately vortexed. Four different dye concentrations were added to the solutions (Scheme 2), namely 14, 7.5, 3.5 and 1.5 × 10^{-3} M. The particles were centrifuged (three times at 1 min, 10,000 rpm) after rotating for another 2 h, washed twice with 1.5 mL of Milli-Q water and once with absolute ethanol and dried in a vacuum oven overnight at room temperature to obtain **D**-doped **PS40** (**D-PS40**). Only THF was added to prepare a blank solution.

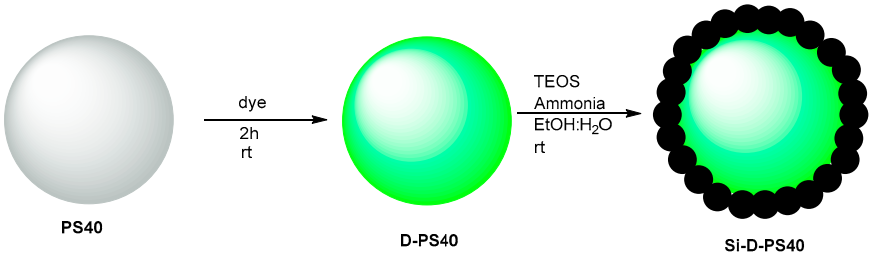

Scheme 2. A schematic representation of dye doping and silica coating of the **PS40** particles. **D** = azaBODIPY dyes **1** or **2**; and TEOS = tetraethylorthosilicate.

*2.6. Coating of **PS40** with Silica Shell*

About 10 mg of the **D-PS40** particles were weighed in Eppendorf tubes and suspended in 1 mL of absolute ethanol. About 20 µL of Milli-Q water was added. The suspension was sonicated for a few minutes and then vortexed. An amount of 30 µL of TEOS and ammonia was added, and the solution was vortexed (Scheme 2). The particles were left to mix at room temperature for 20 h in a Thermomixer. The suspension was washed by centrifugation (10 min, 6000 rpm) three times in Milli-Q water with subsequent removal of the supernatant. The silica-coated **D-PS40** (**Si-D-PS40**) particles prepared in this manner

were dispersed in 5 mL of 70% ethanol using a vortex followed by centrifugation. This was repeated twice for 5 min, and each time the supernatant was removed. The particles were then put in the oven to dry overnight.

2.7. Functionalization with APTES and COOH Groups

For the functionalization with amino groups (Scheme 3), ca. 20 mg of the **Si-D-PS40** particles were dispersed in 800 µL of ethanol. A total of 400 µL of a 1 M HCl solution in ethanol was added to activate the surface of the particles, and the mixture was sonicated for 5 min. The particles were washed twice with 400 µL of ethanol and dispersed in 400 µL of ethanol. Then, 4 µL of APTES was added for amino modification, and the mixture was left to react in a Thermomixer (500 rpm) at room temperature overnight. The amino-functionalized **Si-D-PS40** (**NH_2-D-PS40**) particles prepared in this manner were washed three times with an EtOH:H_2O mixture (1:1). Then, they were dried in vacuo at room temperature.

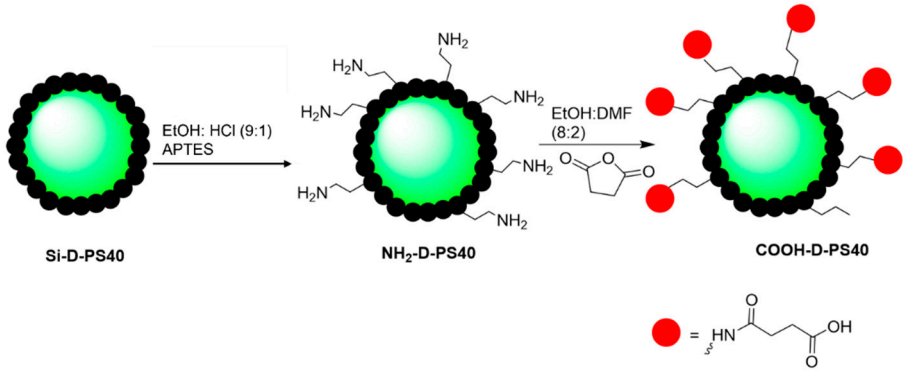

Scheme 3. Functionalization of **Si-D-PS40** particles with APTES, and subsequently with carboxylic acid groups.

For the preparation of carboxylic-acid-substituted **Si-D-PS40** particles (**COOH-D-PS40**) particles, 5 mg of the corresponding **NH_2-D-PS40** amino group-modified particles were dispersed in 1.5 mL of ethanol by using 2 mL Eppendorf tubes. Then, 30 µL of succinic anhydride in DMF (10%, 10 mg in 100 µL) was added, and the mixture was left to react in a thermomixer (800 rpm) at room temperature overnight. Then, the particles were washed three times with an EtOH:H_2O mixture (1:1). In the last step, 500 µL of ethanol was added to provide the final concentration of 1% (*w*/*v*) as a stock solution.

2.8. Coupling with c-HPV and Hybridization Assay

For the coupling of c-DNA to the **COOH-D-PS40** particles (Scheme 4), 10 µL of 1% (*w*/*v*) stock solution of **COOH-D-PS40** particles was dispersed in 200 µL of MES buffer (pH 5, 0.1 M). To this dispersion, 80 µL of a freshly prepared EDC solution and 160 µL of an NHS solution in MES buffer were added. After being left for 15 min at room temperature, 12 µL of a 0.1 mM c-HPV solution was added, and the mixture was left to react in a Thermomixer (1000 rpm) at room temperature overnight to obtain the c-HPV coupled particles (**c-HPV-D-PS40**). 200 µL of Tris/SDS buffer (0.1 M Tris-HCl with 0.05% SDS) was added, and after centrifugation, the mixture was washed twice with 1000 µL of Tris/SDS (0.1 M Tris–HCl with 0.05% SDS). Finally, the particles were dispersed in 200 µL of 0.1 M Tris–HCl $MgCl_2$ (pH 8) to reach a stock solution concentration of 0.025%.

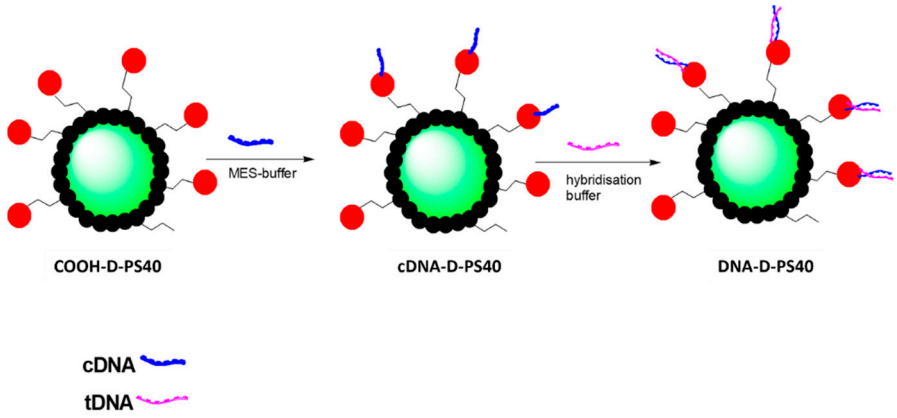

Scheme 4. A schematic representation for the covalent bonding of the c-DNA to the **COOH-D-PS40** particles in the first step, and in the second step hybridization with the t-DNA.

For the hybridization assays, 5 µL of the c-HPV modified stock solution was mixed with 95 µL of hybridization buffer. A total of 5 µL of the complementary t-HPV was added at concentrations of 2, 0.2, 0.1, 0.02, 0.01, 0.002, 0.0002, 0.00002 and 0.00001 pmol/µL along with a blank measurement with no t-HPV. The hybridization buffer was a mixture of Tris (50 mmol) and $MgCl_2$ (80 mmol) in water (pH 8).

2.9. Ninhydrin Test

The ninhydrin test (Scheme 5) was used to quantify amino groups (Table 1) by following the protocol of Soto Cantu et al. [31]. A total of 5 mg of amino-functionalized particles were dispersed in 1.4 mL of ethanol, and 0.4 mL of a ninhydrin solution (0.35%) was added. The reaction was carried out in a Thermomixer at 65 °C and 10 rpm over 2 h. Upon cooling, the mixture was centrifuged, and 0.5 mL of the supernatant was diluted with 1.5 mL of ethanol. The absorbance of the solution was measured on a Specord 210 plus spectrophotometer from Analytik Jena.

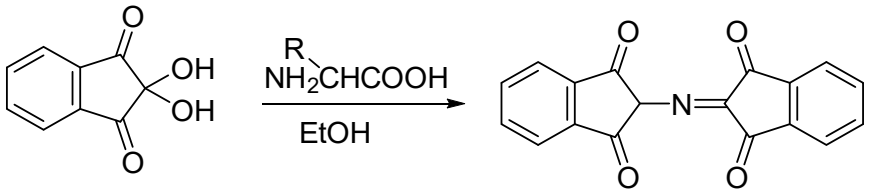

Scheme 5. A schematic representation of the ninhydrin reaction.

Table 1. Concentrations of the amino groups on the **NH_2-D-PS40** particles.

NH_2-D-PS40	Absorbance	Conc. (mM)	Mass (mg)	Conc. (mM g^{-1}) ($\times 10^{-5}$) [1]
NH_2-1-PS40	2.3×10^{-2}	6.0×10^{-2}	1	6.0
NH_2-2-PS40	1.3×10^{-2}	2.4×10^{-2}	1	2.4
NH_2-B-PS40	5.3×10^{-3}	2.2×10^{-2}	1	2.2

[1] M/g = number of moles per mass of supporting particles.

3. Results and Discussion

3.1. Synthesis and Characterization

Experiments were performed using **PS40** polystyrene particles produced according to our established protocol [11]. The **PS40** particles were stabilized by poly(vinylpyrrolidone) (PVP) with an average molecular weight of ca. 40 kDa. PVP also acts as a capture agent, promoting precipitation of silica seeds on the surface which are further overgrown during the shell formation step [32,33]. The polystyrene particles had a diameter of 2.5 µm. The

relatively large surface area provides a desirable environment for enhancing reaction kinetics and enables the use of small reaction volumes. Unfunctionalized hydrophobic azaBODIPY dyes **1** and **2** were used to encode the **PS40** particles (Figure 1).

To confirm the successful doping of **PS40** beads with the azaBODIPY dyes, fluorescence spectra of **1** and **2** of the particles were measured at excitation wavelengths of 650 and 700 nm in ethanol, respectively, at a concentration of 1.0 µM. As shown in Figure S3 in the Supplementary Material, when the dye is incorporated in the **PS40** beads, blue shifts of 12 and 5 nm are observed in the emission spectra of **1** and **2**, respectively, since azaBODIPYs are known to be solvatochromic [34]. The environment of the dye differs markedly in the **PS40** beads from that in ethanol solution. The light scattering properties of the polystyrene beads may also have an influence, as reported by Lagorio et al. [35]. They showed that the scattering of light can lead to light re-absorption processes, which produce emission spectral distortions depending on the layer thickness of the fluorescent material, sample absorption at the excitation and emission wavelengths, and the excitation wavelength. As expected, no emission was observed for the undoped **PS40** beads.

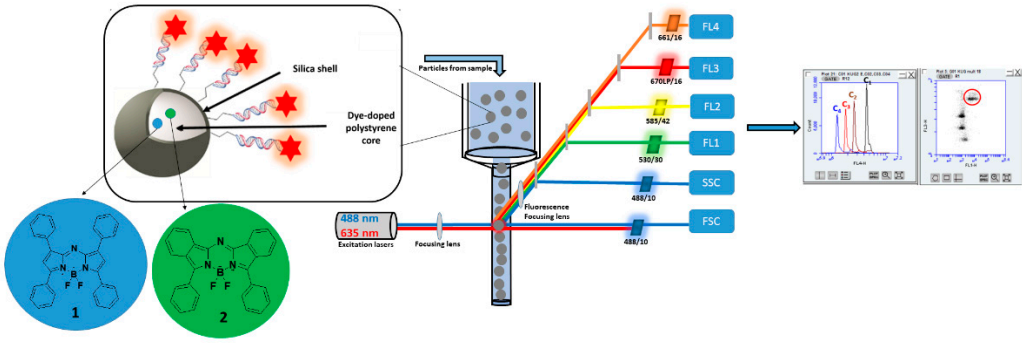

Figure 1. Schematic diagram of a dye-doped and silica-coated polystyrene core-shell particle functionalized with DNA strands [11] (left), a typical flow cytometer measurement cell (middle), highlighting the hydrodynamic focusing of the single particles and their optical interrogation via scattering (forward, FSC, 180° geometry; sideward, SSC, 90° geometry) and fluorescence channels (FL1-FL4) [36], and typical measurement results (right; histogram, density dot plot).

The doping of **PS40** particles was carried out in THF, and the particles were washed twice with ethanol in dispersion/centrifugation cycles. For further modification, the azaBODIPY dye-doped **PS40** particles were redispersed in an ethanol:water mixture functionalization medium to prepare a stock concentration of 1% w/v. The formation of a hydrophilic silica shell on the surface of the **PS40** particles was achieved by following an ammonia-catalyzed sol–gel process with TEOS as a precursor. Since the aim of this work was to use the particles produced in DNA hybridization assays as carriers for the target strands, further functionalization of the silica shell was vital. Aminopropyltriethoxysilane was condensed on the surface of the core/shell particles, to provide amino groups as anchors for further conjugation in a ring-opening reaction with succinic anhydride to form carboxylic acid moieties on the surface (**COOH-D-PS40** in Scheme 3). In order to quantify the amino groups on the surface of the **NH_2-D-PS40** particles, a ninhydrin test was carried out. In this test, primary amines react with ninhydrin and produce the dye Ruhemann's Purple, which has an absorption maximum at 580 nm [37]. Spectra of the colored supernatant of the suspension were measured with a spectrophotometer. A calibration curve was obtained with pentylamine which is provided in Figure S4 of the Supplementary Material. Table 1 provides the concentration of the amino groups in mM in solution and in $mM.g^{-1}$ of solid. The concentration of the amino groups was found to be around 2.19, 6.04 and 2.43 $\times$ 10^{-5} mM g^{-1} for the blank non-doped particles (**NH_2-B-PS40**), dye-doped **NH_2-1-PS40** and **NH_2-2-PS40** particles, respectively.

As can be observed in Figure S4B in the Supplementary Information, azaBODIPY **1** leached out at 65 °C during the ninhydrin test experiment. To avoid this, all experiments

were carried out at room temperature. The low concentration of amino groups on the surface of these particles compared to values reported in the literature [14] could be due to an incomplete formation of the shell and/or because the SiO_2 coating did not result in a shell with a significantly increased surface area. The different elements present in both the blank and doped particles were confirmed by EDX analysis. As shown in Figure 2A, the EDX data for the bare **PS40** particles (left) contain strong peaks for carbon and oxygen atoms from the polystyrene core. The presence of Si, B, N, O and F peaks confirms the successful adsorption of the azaBODIPY dyes and the presence of silica coating (Figure 2B, right). In addition, the high carbon content in the silica shelled particles can be attributed to the diffusion of PVP chains of the polymeric core into the shell layer via capillary forces due to the small size of the SiO_2 seeds on the surface [38].

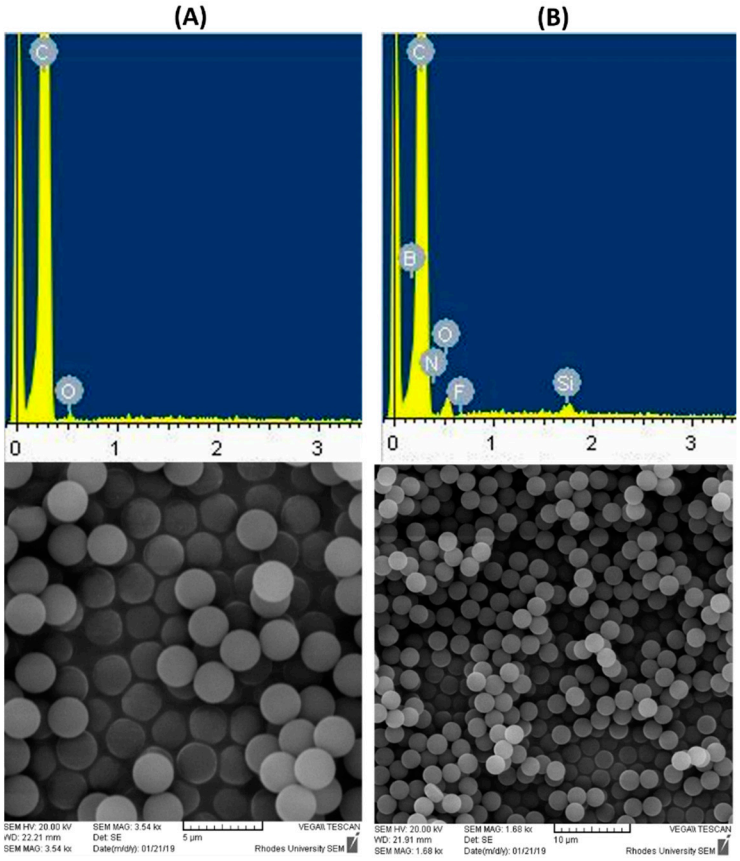

Figure 2. EDX spectra and SEM images of (**A**) **PS40** (left) and (**B**) azaBODIPY dye-doped and silica-coated **PS40** particles (right).

SEM was used to view the morphology of the particles and to determine their diameters (Figure 2). The SEM images were processed by ImageJ [39], a freely available open-source software. The projection area of individual particles was determined using ImageJ's built-in analysis tool. Statistical analysis of all counted particles was carried out to calculate the mean diameter size and the standard deviation (σ). The doped particles had an average diameter of 2.50 ± 0.03 µm, whereas the average value for the doped silica-coated particles was 2.55 ± 0.03 µm, implying a shell thickness of ca. 0.025 µm. This increase in the particle size is consistent with successful coating of the particles. The size distribution can be described with a coefficient of variation (C_v), which corresponds to the ratio of the standard deviation to mean size (χ_m). The coefficients of variation ($C_v = \sigma/\chi_m$) for the doped and doped silica-coated particles amounted to 1.6 and 1.5%, respectively. Since these values are less than 5%, an acceptable level of monodispersity was achieved.

This is of great importance for comparability and data interpretation in suspension array technologies (SATs), especially with regard to cytometric assays [40].

Different silica shell morphologies can be obtained depending on the synthetic strategy. Water-based emulsifier-free emulsion techniques can be used to prepare positively or negatively charged polymeric core templates [38]. In this work, negatively charged polymer cores were synthesized. Figures 3 and 4 show the TEM images of the uncoated, silica-coated, and APTES and COOH functionalized particles. The coated particles show an assembly of small silica nanoparticles fused together to varying degrees to form the shell. The particle morphology is rougher in appearance for the coated particles compared to the uncoated particles (Figures 3 and 4).

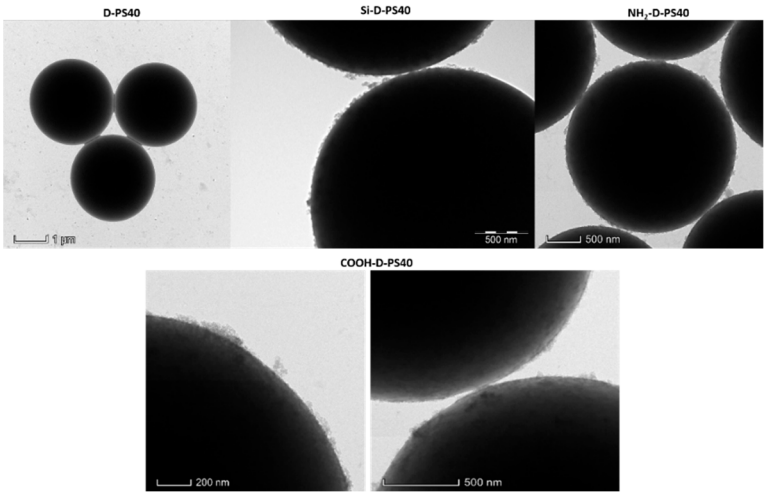

Figure 3. TEM images of doped **PS40**, silica-coated, and APTES and COOH functionalized **PS40** particles.

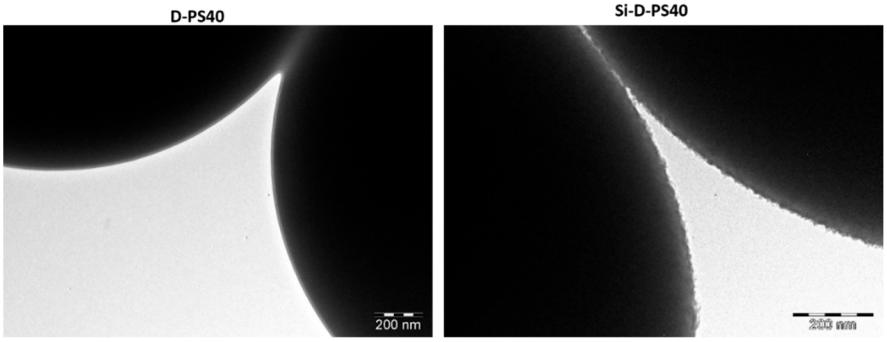

Figure 4. TEM images of doped **PS40** and doped silica-coated **PS40** particles showing unmodified and modified surfaces.

Thermogravimetric analyses were performed for azaBODIPY **1** and the **D-PS40**, **Si-D-PS40** and **NH_2-D-PS40** particles under a nitrogen atmosphere to determine the success of the functionalization. The decomposition temperature was found to increase with the functionalization of the particles. The decomposition temperature (T_d) values obtained at a 5% weight loss were ≈199 ± 1 °C for azaBODIPY **1**, ≈239 ± 1 °C for **D-PS40**, ≈ 304 ± 1 °C for **Si-D-PS40** and ≈341 ± 1 °C for **NH_2-D-PS40** (Figure 4). The TGA profiles of the particles also reveal three phases which can be assigned to the following processes: up until ≈280 ± 1 °C, water desorption takes place (phase 1) followed by core burning until ca. 450 °C (phase 2) [32]. In the third phase, condensation reactions and removal of organic residues from the silica domain occur until only the inorganic SiO_2 remains [41]. The SiO_2 content was estimated to be 1.6%, which is consistent with the presence of a thin

silica shell as would be anticipated based on the TEM images, the low silicon composition observed by EDX and the small diameter increase of the particles in the SEM images. The T_d value for azaBODIPY **1** increased from 170 to 288 °C when doped onto the polystyrene bead, which implies that there is enhanced thermal stability in this context (Figure 5).

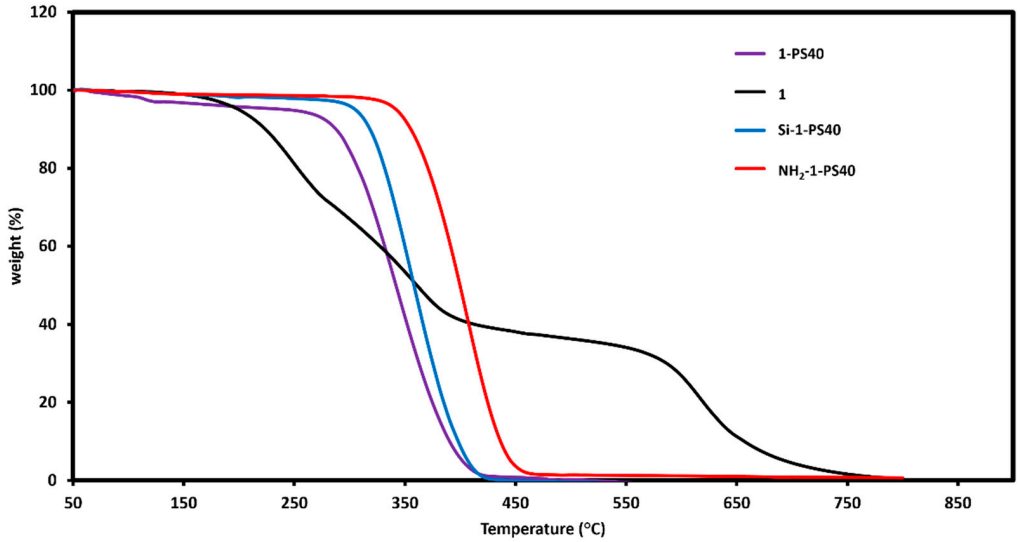

Figure 5. TGA profiles of **1-PS40**, **1**, **Si-1-PS40** and **NH_2-1-PS40** at a heating rate of 20 °C min^{-1} under a nitrogen atmosphere.

3.2. Characterization of the Particles in Flow Cytometry

To characterize the particles by flow cytometry, dynamic light scattering was used to gain insight into their size, granularity and the overall outside structure of the particles by measuring the forward (FSC) and sideward scattering (SSC). The FSC correlates with the volume of the particles and is a measure of the diffraction of the light at a flat angle, whereas, with SSC, the scattering of the light is detected at right angles. Larger particles with an uneven surface lead to high values for FSC and SSC, while smaller particles with an even surface result in lower values. To investigate the potential utility of the doped silica-coated particles as SAT elements, their scattering properties were compared to those of the bare core particles. The difference in size should be significant to enable successful detection by cytometry.

There is an increase in the FSC and SSC intensities on moving from blank **PS40** particles to the silica-coated particles, which further increases upon functionalization with APTES to obtain NH_2 functional groups (Table 2). The statistical analyses of these measurements in Table 2 show the differences in the C_v values before and after silica coating. Values of more than 5% were obtained for both uncoated and silica-coated particles, indicative of less monodispersed particles. However, the monodispersity improves slightly upon functionalization with APTES, as indicated by the decrease in the C_v values.

Table 2. Statistical analysis of the scattering properties of unmodified and modified **PS40** particles.

	Mean FSC-H ($\times 10^5$)	**C_v FSC-H (%)**	**Mean SSC-H ($\times 10^5$)**	**C_v SSC-H (%)**
Blank	2.27	7.8 (±0.39)	3.47	11.8 (±0.59)
Si-1-PS40	2.49	8.2 (±0.41)	4.36	11.5 (±0.58)
Si-2-PS40	2.39	11.8 (±0.59)	3.97	11.4 (±0.57)
NH_2-Blank	2.62	7.4 (±0.37)	3.86	10.7 (±0.53)
NH_2-1-PS40	2.67	7.2 (±0.36)	3.89	10.8 (±0.54)
NH_2-2-PS40	2.78	6.7 (±0.34)	3.88	10.9 (±0.55)

Figure 6 contains histogram plots obtained in flow cytometry measurements for the uncoated, silica-coated, and APTES and COOH functionalized **PS40** particles doped with azaBODIPYs **1** and **2** (Figure 6). This plot provides qualitative information on the properties of the particles, such as their size distributions and the presence of secondary particles with high-intensity values. In the histogram plot, three different regions can be identified; the main peak centered at the peak maximum ($\chi_m \pm 3\sigma$, derived from a Gaussian fit), secondary particles at lower values ($<\chi_m - 3\sigma$) and aggregated particles at higher values ($>\chi_m + 3\sigma$). For the **1-PS40** particles, a bell-shaped distribution was observed with both secondary particles at lower FSC-H values and aggregated particles at higher FSC-H values. In contrast, the histogram plot of **2-PS40**-doped particles showed a slightly left-skewed distribution with secondary particles at lower FSC-H values. A right-skewed distribution was observed upon modification of the doped **PS40** particles with silica, APTES and COOH, with the data lacking any hint of smaller secondary particles.

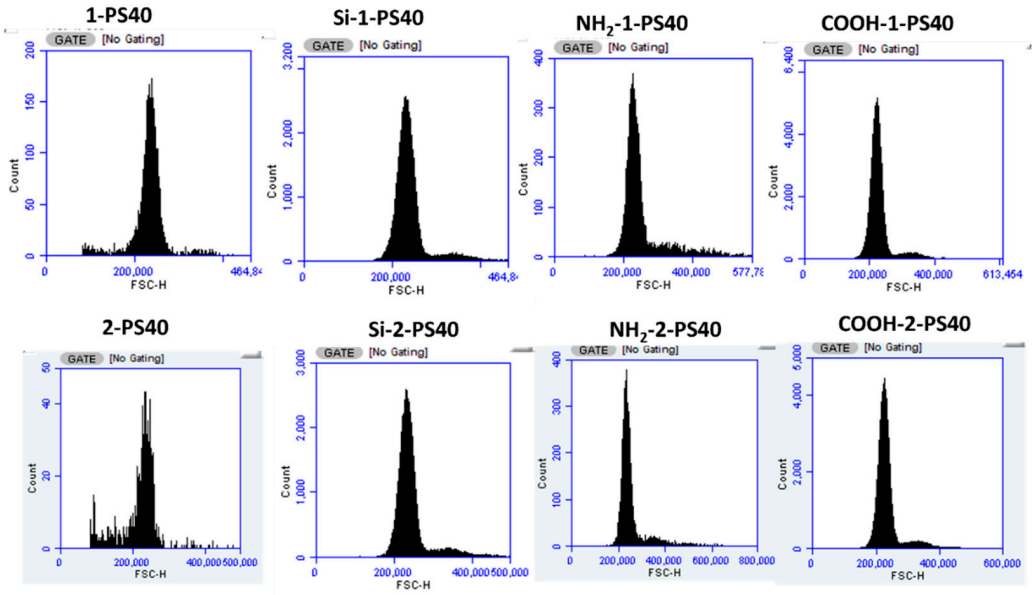

Figure 6. Histogram plots for the single particle flow cytometric analyses of **1-PS40**, **Si-1-PS40**, **NH_2-1-PS40** and **COOH-1-PS40** (top); **2-PS40**, **Si-2-PS40**, **NH_2-2-PS40** and **COOH-2-PS40** (bottom).

3.3. HPV Detection Using Flow Cytometry

For HPV detection studies, three structurally different dyes were used, and four concentrations of each were prepared. However, problems can be encountered when using dyes as a color code to generate larger library codes, including spectral cross-talk or concentration quenching. In this work, these can be neglected since the dyes were sterically loaded into the PS core by swelling [42–45]. BODIPY dyes [43,45] are excellent candidates for this application due to their photostability and bright color. In this context, azaBODIPY dyes were applied for the first time following the dye encoding procedure for PVP-stabilized PS cores shown in Scheme 2. The following concentrations were prepared: **C_1** = 14 mM, **C_2** = 7 mM, **C_3** = 3.5 mM and **C_4** = 1.75 mM in THF. All particle population distributions are well resolved in the fluorescence histogram plots (FL1-H and FL3-H and/or FL4-H) and the correlation plot between FL1-H and FL3-H (Figure 7). Figures 7–9 show a dot and histogram plot for the doped (**D-PS40**) and the COOH functionalized (**COOH-D-PS40**) particles. **1** and **2** emit red fluorescence at 672 ± 13 and 731 ± 14 nm, respectively, at excitation wavelengths of 650 and 700 nm. This matches the optical layout of the conventional benchtop cytometer that was used (Figure 1). As shown in Table S2 in the Supplementary Material, the **D-PS40** lost some of the dye they were coded with initially. The red boxes inside the dot plots highlight the location of the doped **PS40** particles before the formation of the silica shell (Figure 7A).

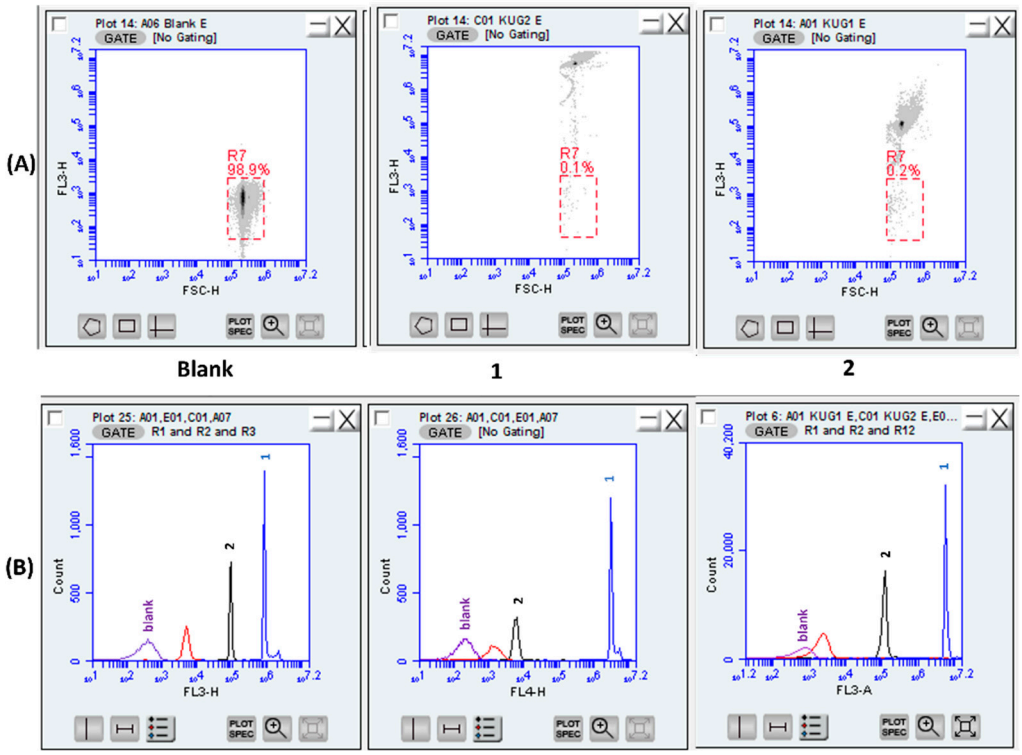

Figure 7. (**A**) Dot plots for the single particle flow cytometric analysis for (left to right) **Blank**, **1-PS40** and **2-PS40**. (**B**) Fluorescence plots for the (left to right) **Blank**, **1-PS40** and **2-PS40** analyzed at FL3-H and FL4-H channels, respectively.

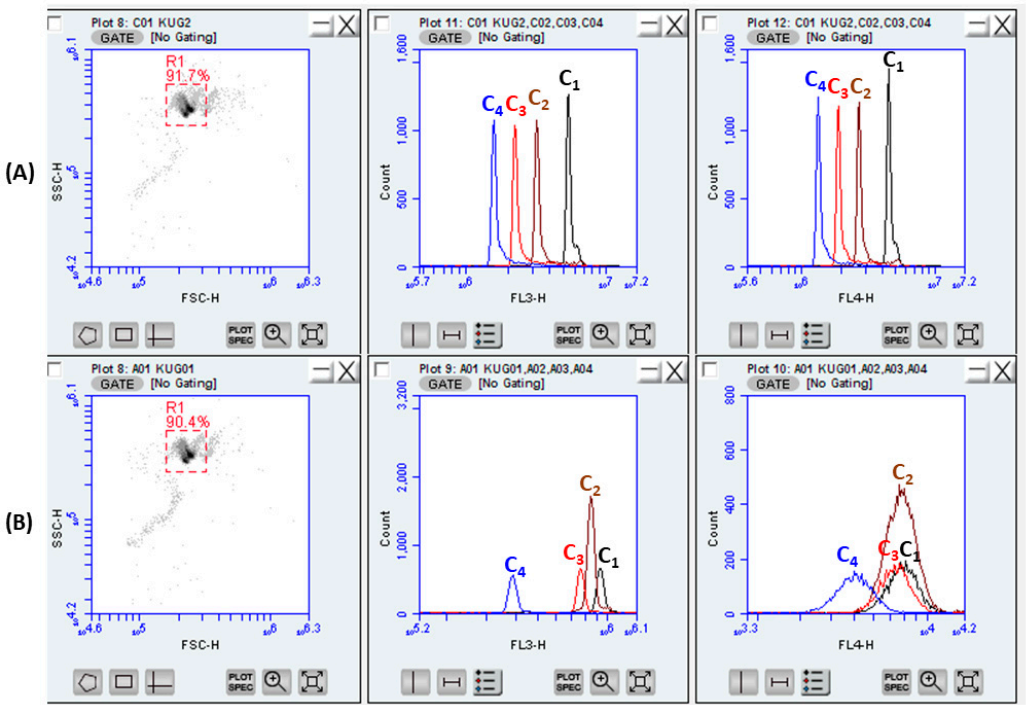

Figure 8. Characterization of a single particle flow cytometric analysis of (**A**) **1-PS40** and (**B**) **2-PS40** showing dot plots (left) and the separation in the fluorescence of the four different concentrations of each of these dyes in the FL3-H and FL4-H channels (middle and right). The red boxes inside the dot plots highlight the location of the doped **PS40** particles before the formation of the silica shell.

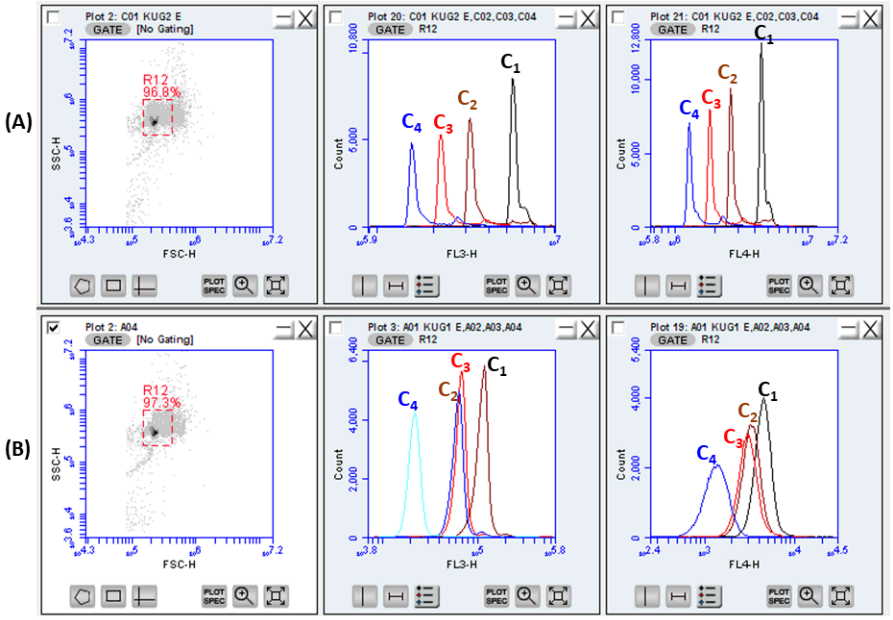

Figure 9. Characterization of a single particle flow cytometric analysis of (**A**) **COOH-1-PS40** and (**B**) **COOH-2-PS40**, showing dot plots (left) and the separation in the fluorescence of the four different concentrations of each of these dyes in the FL3-H and FL4-H channels (middle and right).

The flow cytometry was measured after each step during the synthesis and modification of the doped **PS40** silica-coated particles to monitor the separation in the fluorescence of the four different concentrations prepared for each dye. Figures 8 and 9 show the results obtained for all the dyes after doping and functionalization with the COOH groups of the **PS40** particles. As shown in Figures 8 and 9, both the doping and COOH steps of the particles doped with **1** resulted in an acceptable separation of the concentrations from highest to lowest with both layers and as expected, the fluorescence increased with dye concentration (Figures 8A and 9A). The highest and the lowest concentrations were well separated upon doping with **2**, but the middle two concentrations were not (Figures 8B and 9B). These results could be due to the leaching out of **2** during the reaction and/or washing stage.

3.4. Hybridization Assays

The hybridization assays were performed using different strands of c-DNA. HPV18, HPV16, HPV11 and HPV6 were attached to the particles through EDC-mediated coupling. A c-DNA with an amino group at the 5′-position was covalently bound to **COOH-D-PS40**, where **D** represents azaBODIPYs **1** and **2**. The **c-DNA-D-PS40** was hybridized with the corresponding t-DNA complementary strand, and the suspension of **c-DNA-D-PS40** was then measured on the cytometer. To prepare for the hybridization and multiplex assay experiments, the **PS40** particles doped with $\mathbf{C_1}$, $\mathbf{C_2}$, $\mathbf{C_3}$ and $\mathbf{C_4}$ concentrations of azaBODIPYs **1** and **2** were covalently linked with HPV18, HPV16, HPV11 and HPV6 DNA strands, respectively (Table 3). Each concentration contained a different c-DNA strands that were mixed with the corresponding t-DNA. Nine different concentrations of the t-DNA were prepared, and upon mixing with **c-DNA-D-PS40** particles, the fluorescence properties of the particles were measured in flow cytometry. The results obtained are presented in Figure 10 and Figure S5 in the Supplementary Material, with **c-DNA-1-PS40** provided as an example. The fluorescence measured in the FL1-H channel corresponding to the 6-carboxyfluorescein (FAM) labeled, complementary t-DNA strand increased with the concentration of t-DNA added to each **c-DNA-D-PS40** particle. As expected, only one signal was observed in the FL3-H channel during this titration, this channel identifying the c-DNA sequence through the unique dye and concentration that have been used for

doping the **PS40** core. The data in Figures 10 and S5 were used to plot the calibration curves presented in Figures 11 and 12.

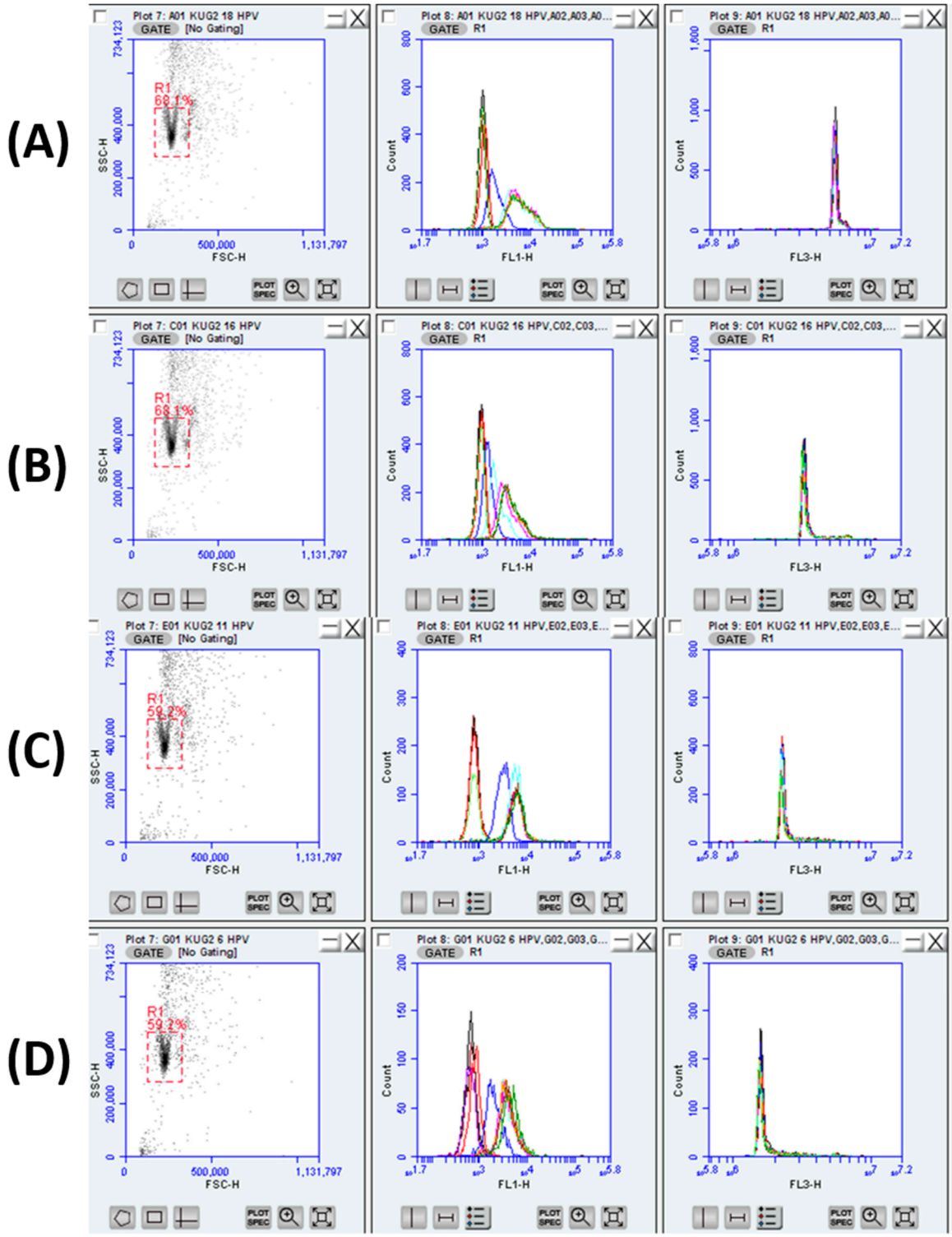

Figure 10. Flow cytometry measurements for the 1:1 hybridization assay of complementary FAM-labeled t-DNA towards the C1-C4 concentrations of (**A**) **c-DNA18-1-PS40**, (**B**) **c-DNA16-1-PS40**, (**C**) **c-DNA11-1-PS40** and (**D**) **c-DNA6-1-PS40** particles at the nine different concentrations shown in Figure 11 of the strand complementary to the target, showing dot plots (left) and the fluorescence measured in the FL1-H (middle) and FL3-H (right) channels highlighted with a series of different colors.

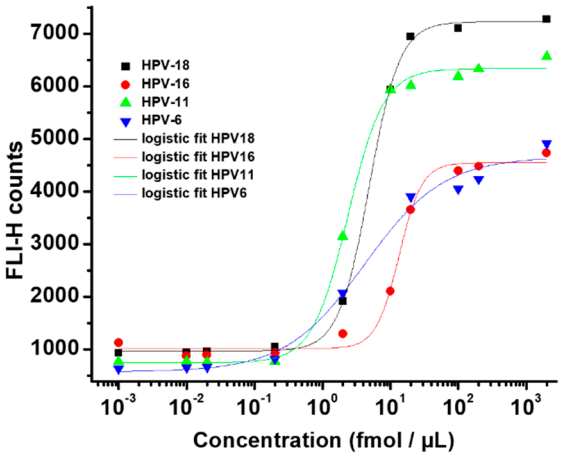

Figure 11. Calibration curves for the hybridization of complementary FAM-labeled t-DNA towards **c-DNA-1-PS40** particles using nine concentrations of the strand complementary to the target. A logistic function was used to fit the data and to extract the linear range (EC_{20} to EC_{80}) and the limit of quantification (LOQ, EC_{20}).

Table 3. Details of the hybridization assays with azaBODIPYs **1** and **2**.

Concentration of Dye Added (mM)	HPV c-DNA Strand Added	Name of Material
C_1 = 14	HPV-18	**c-DNA18-1-PS40**
C_2 = 7	HPV-16	**c-DNA16-1-PS40**
C_3 = 3.5	HPV-11	**c-DNA11-1-PS40**
C_4 = 1.75	HPV-6	**c-DNA6-1-PS40**
C_1 = 14	HPV-18	**c-DNA18-2-PS40**
C_2 = 7	HPV-16	**c-DNA16-2-PS40**
C_3 = 3.5	HPV-11	**c-DNA11-2-PS40**
C_4 = 1.75	HPV-6	**c-DNA6-2-PS40**

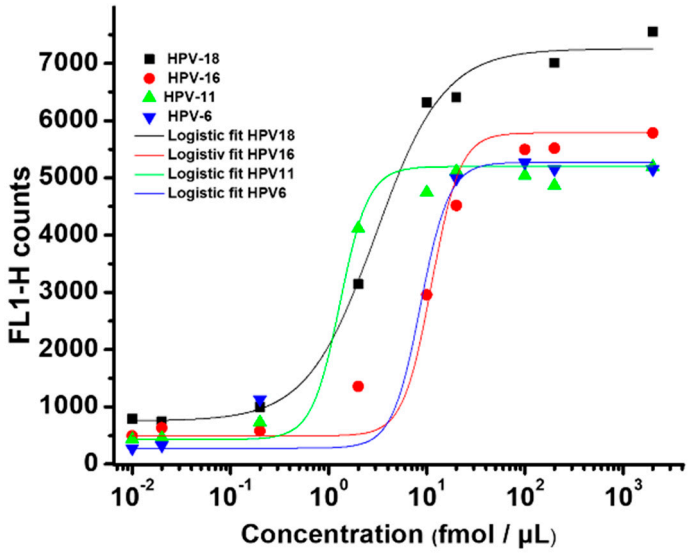

Figure 12. Calibration curves for the hybridization of complementary FAM-labeled t-DNA towards **c-DNA-2-PS40** particles using nine concentrations of the strand complementary to the target. A logistic function was used to fit the data and to extract the linear range (EC_{20} to EC_{80}) and the limit of quantification (LOQ, EC_{20}).

The sensitivities of the model assays using **D-PS40** particles were compared to those of existing techniques by determining the limit of detection (LOD) values. For example, Horejsh et al. derived the LOD value as the background signal plus 10σ and found values of ca. 30 fmol for a molecular beacon-based, amplification-free direct binding assay without washing [46]. On the other hand, Thiollet et al. used quantum-dot encoded microspheres and determined similar detection limits but had to perform several washing steps after hybridization [47]. Sarma et al. [11] reported an LOD of < 1 fmol, i.e., ca. 0.1–0.2 fmol without extra washing. In addition to quantifying the LOD, logistic regression can be used to determine the limit of quantification (LOQ) and define the linear range to adequately describe the hybridization assay performance of the materials.

In this study, a logistic function was used to fit the data and to obtain the linear range (EC_{20} to EC_{80}) and the limit of quantification (LOQ, EC_{20}). The data obtained for the 1:1 assays in this study are summarized in Table 4, and the calibration curves are shown in Figures 11 and 12. **c-DNA16-1-PS40, c-DNA18-1-PS40**, **c-DNA6-2-PS40 and c-DNA16-2-PS40** had LOD values > 5 fmol μL^{-1}, while values < 1 fmol μL^{-1} were obtained for **c-DNA11-1-PS40**, **c-DNA6-1-PS40, c-DNA18-2-PS40** and **c-DNA11-2-PS40**. Therefore, both types of particles exhibit very high sensitivity towards the detection of **c-DNA11.** These LOD values are slightly higher than what has been reported previously for other similar systems mentioned above. In comparison to the ELISA and microarray assay, however, which have LODs ranging from 1 pg/mL to 10 nm/mL [18,48–51], SAT-based assays exhibit higher sensitivity with LOD values in the 0.1−5 fmol μL^{-1} range and lower [11,12,14].

Table 4. LOD values, LOQ values and linear ranges for **c-DNA-1-PS40** and **c-DNA-2-PS40**.

c-DNA-1-PS40	**HPV18**	**HPV16**	**HPV11**	**HPV6**
LOD (fmol μL^{-1})	1.47	6.64	0.78	0.83
LOQ (fmol μL^{-1})	1.09	7.45	1.40	5.41
Linear range (fmol μL^{-1})	2.4−10	7.8−23.0	1.0−5.5	0.66−2.50
c-DNA-2-PS40	**HPV18**	**HPV16**	**HPV11**	**HPV6**
LOD (fmol μL^{-1})	0.22	5.27	0.67	4.72
LOQ (fmol μL^{-1})	3.36	4.46	3.14	9.40
Linear range (fmol μL^{-1})	0.99−9.01	7.04−17.7	0.82−2.07	5.4−13.7

The LOQ values were also relatively low for **c-DNA18-1-PS40**, **c-DNA11-1-PS40**, **c-DNA18-2-PS40** and **c-DNA11-2-PS40**. On the other hand, the detection ranges (represented as the linear range in Table 4) of the assays were determined to lie between 0.99−23 fmol μL^{-1}, a relatively narrow range. This could have a beneficial impact if the measurements are carried out at lower concentrations.

3.5. Multiplexed Assays

After optimizing the parameters of each assay separately in a nonmultiplexed format, the assays were multiplexed by preparing several particles containing different DNA strands. For these assays, the main focus was on **c-DNA-1-P40** because it had met the requirement of having a fluorescence signal that lies in a different region than that of the 6-FAM marker that was used to label the t-DNA with peaks for the different concentrations that are well separated. The monodispersity was maintained after the incorporation of all the dye concentrations, as shown by the dot plots presented in Figures 9, 10, 13 and 14. Since the **c-DNA-1-PS40** particles contain four different concentrations, four batches are present in the FL3-H fluorescence channel (Figure 13F). The 4:1 assay presented in Figure 13 shows the fluorescence of the particles plotted against the green fluorescence (FL1-H) corresponding to the complementary c-DNA used in a dot plot for the four batches.

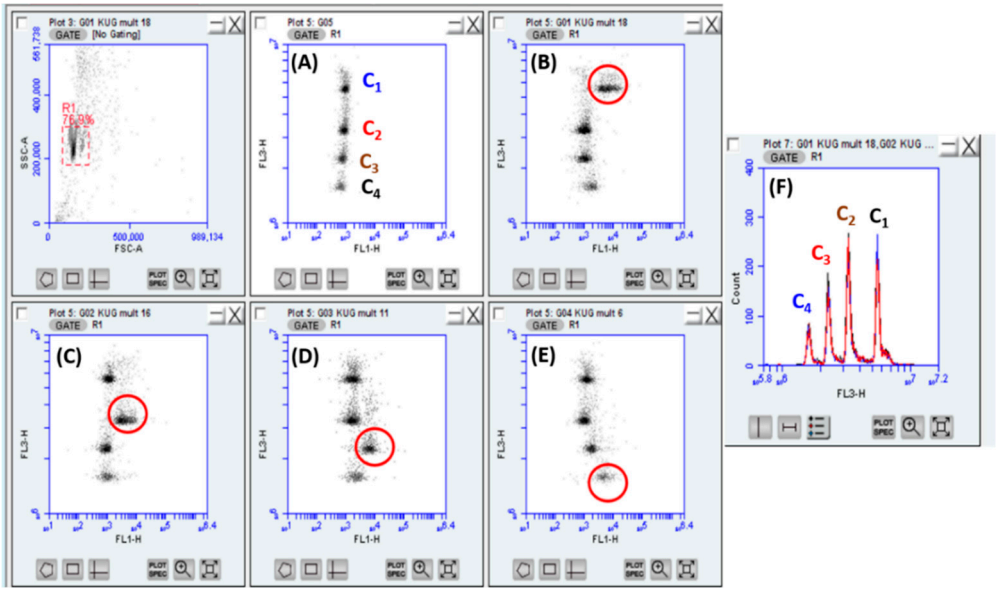

Figure 13. Flow cytometry measurements of the 4:1 multiplex assay with **c-DNA-1-PS40**. (**A**) The assay response to the particles free of HPV t-DNA strands. (**B**–**E**) The assay response in the presence of the HPV18, HPV16, HPV11 and HPV6 t-DNA strands, respectively. The detected t-DNA is highlighted with a red circle. (**F**) The signal in the FL3-H fluorescence channel for the **c-DNA-1-PS40** particles doped with four different concentrations of **1**.

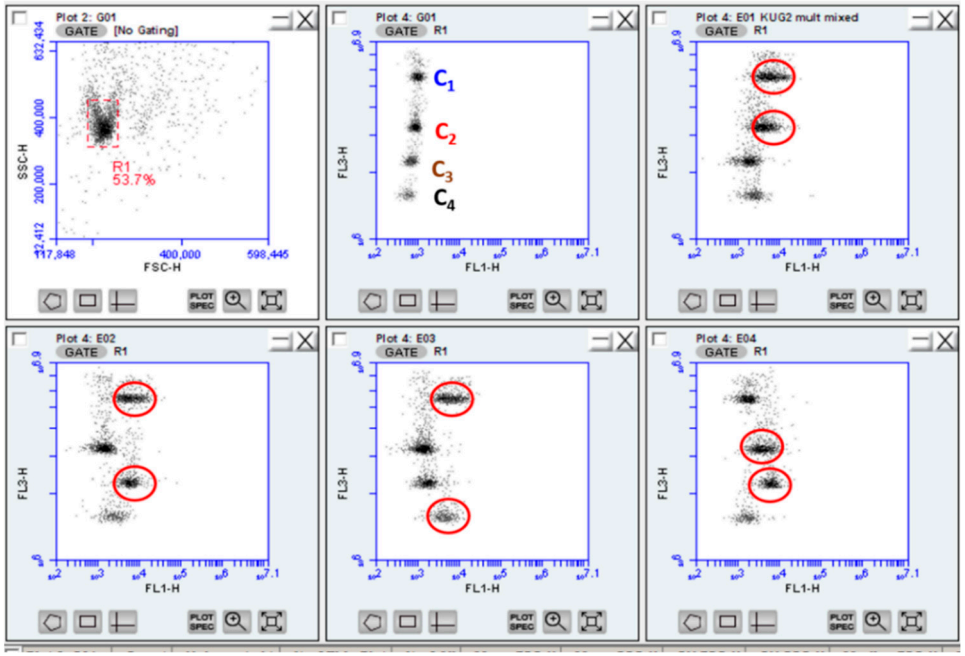

Figure 14. Flow cytometry measurements of the 4:2 multiplex assay with **c-DNA-1-PS40**. The detected t-DNA is highlighted with a red circle.

The first experiment that was performed involved a 4:1 assay format, in which a mixture of the four types of particles containing the four different c-DNA strands for the determination of different HPV species was mixed in a solution containing only one type of t-DNA strand. Figure 13B shows the mixture for the incubation of particles only in the presence of HPV18 t-DNA (encoded with the highest dye concentration). Figure 13C–E shows similar experiments in the presence of only HPV16, HPV11 and HPV6, respectively. An increase in the signal of FL1 was only observed for the coded particles corresponding

to the complementary c-DNA used. This demonstrates that a qualitative analysis of the sample is already possible.

In the second experiment, 4:2 and 4:3 assay formats were performed to further investigate the sensitivity and selectivity of the **c-DNA-1-PS40** particles. Solutions containing two or three types of t-DNA stands were added to a mixture of the four types of particles containing four different c-DNA strands (Figures 14 and 15). Binding of the functionalized c-DNA in the **PS40** particles to the t-DNA enhances the fluorescence (FL1-H). The **c-DNA-1-PS40** particle still shows high sensitivity and selectivity to the two types of t-DNA that are added. However, when three strands were added, the sensitivity was lost in some cases, possibly due to human error. On the other hand, the multiplex assay experiments on the **c-DNA-2-PS40** were unsuccessful (Figure S6 in the Supplementary Material). There was no clear separation in the fluorescence of the particles in the flow cytometry in both FL3-H and FL4-H channels. This was attributed to the loss of some dye in **c-DNA18-2-PS40, c-DNA16-2-PS40** and **c-DNA11-2-PS40** during the washing stages. This could be optimized by using dye concentrations that would ensure a better separation on the cytometry even after the washing stages. Low concentrations would be recommended in this context.

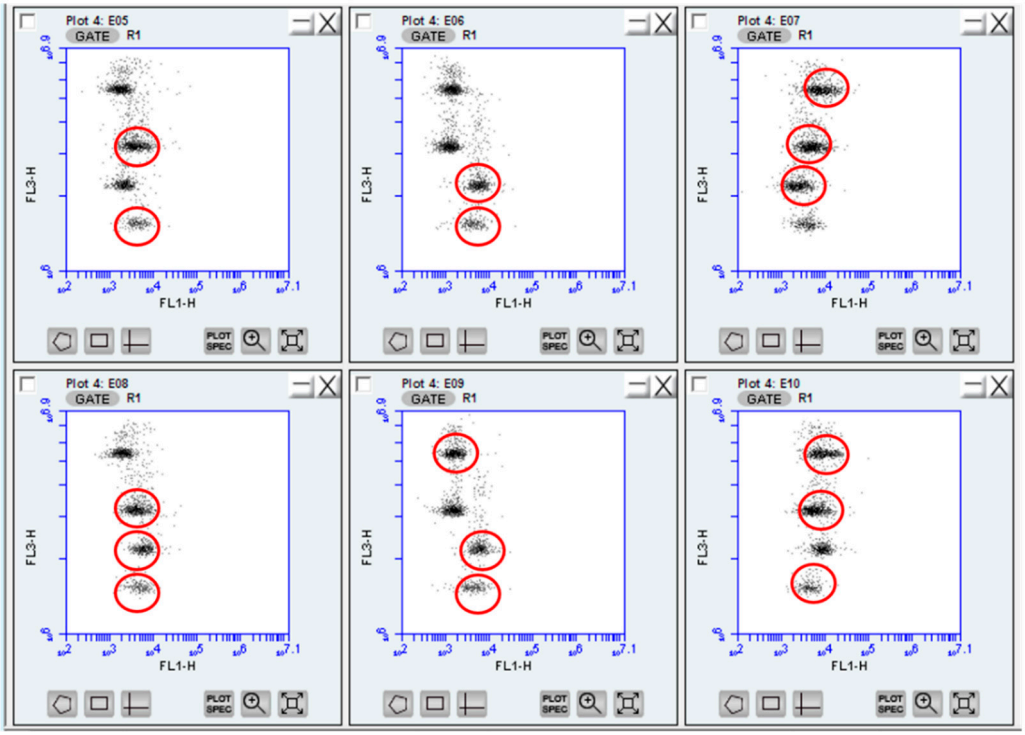

Figure 15. Flow cytometry measurements of the 4:2 and 4:3 multiplex assays with **c-DNA-1-PS40**. The detected t-DNA is highlighted with a red circle.

4. Conclusions

The **PS40** particles were successfully doped with four different concentrations of azaBODIPYs **1** and **2** for use in multiplex assays and were subsequently coated with silica and further functionalized with APTES and then COOH-groups. Flow cytometry, SEM and TEM were used to prove the formation of the **D-PS40**, **Si-D-PS40**, **NH_2-D-PS40**, **COOH-D-PS40** and **c-DNA-D-PS40** particles. The ninhydrin test was used to determine that the concentration of the NH_2 groups in the 10^{-5} M g^{-1} range. There was a clear separation in the fluorescence of the four different concentrations of **1-PS40** measured in the FL3-H and FL4-H fluorescence channels. The FL3-H fluorescence channel gave the best results and was used to study 1:1 hybridization and multiplexed assays. The **c-DNA-1-PS40** and **c-DNA-2-PS40** particles showed low LOD and LOQ values for HPV11,

and a narrow detection range was obtained. The multiplexed assay experiments were successfully performed on **c-DNA-1-PS40** particles, and the results proved that these particles could potentially be used as a tool for multiplexing assays, thus, they merit further in-depth study in this context.

Supplementary Materials: The following supporting information can be downloaded at: https://www.mdpi.com/article/10.3390/chemosensors11010001/s1, Figure S1: 600 MHz ^{1}H NMR spectrum of azaBODIPY **1** in $CDCl_3$; Figure S2: Normalized absorption spectra and emission spectra of azaBODIPYs **1** and **2** in EtOH; Figure S3: Emission spectra of Blank, **1-PS40** and **2-PS40** with excitation wavelengths at 650 and 700 nm in EtOH, respectively; Figure S4: (A) UV-visible absorption spectra and a calibration curve for pentylamine at 580 nm, and (B) absorption spectra of particles functionalized with amino groups (APTES) in the presence of a ninhydrin solution in EtOH; Figure S5: Flow cytometry measurements for the 1:1 hybridization assay of complementary FAM-labeled t-DNA towards the $\mathbf{C_1}$-$\mathbf{C_4}$ concentrations of (A) **c-DNA18-2-PS40**, (B) **c-DNA16-2-PS40**, (C) **c-DNA11-2-PS40** and (D) **c-DNA6-2-PS40** particles at nine different concentrations of the strand complementary to the target, showing dot plots (left) and the fluorescence measured in the FL1-H (middle) and FL3-H (right) channels; Figure S6: Flow cytometry measurements of the 4:1 multiplex assay using **DNA-2-PS40**. (A–D) The assay response in the presence of the HPV18, HPV16, HPV11 and HPV6 t-DNA strands, respectively. (E) The assay response to the particles free of HPV t-DNA strands; Table S1: Photophysical properties of **1** and **2** in different solvents; Table S2: Absorption and concentration of COOH functionalized **Si-PS40** particles. The dye concentration in the particles was also determined using the Beer–Lambert law in EtOH.

Author Contributions: Conceptualization, G.K., E.C. and K.R.; formal analysis, G.K. and E.C.; investigation, G.K., E.C. and C.T.; resources, K.R., J.M. and T.N.; data curation, G.K. and J.M.; writing—original draft preparation, G.K.; writing—review and editing, G.K., E.C., C.T., K.R., J.M. and T.N.; visualization, G.K. and E.C.; supervision, J.M., K.R. and T.N.; project administration, K.R. and J.M.; funding acquisition, J.M., K.R. and T.N. All authors have read and agreed to the published version of the manuscript.

Funding: This research was funded by The Department of Science and Technology (DST) and National Research Foundation (NRF) of South Africa through DST/NRF South African Research Chairs Initiative for Professor of Medicinal Chemistry and Nanotechnology to T.N. (uid: 62620), CSUR, and ISRR grants from the NRF of South Africa to J.M. (uids: 93627 and 119259), a Focus Area Analytical Sciences grant from BAM/BMWK to K.R. (TF-20, MamaLoCA), an Individual Research Grant from German Research Foundation (DFG) to E.C. (CL 761/1-1), and a DAAD-NRF in-country doctoral scholarship to G.K. (uid: 101816) is gratefully acknowledged.

Data Availability Statement: Not applicable.

Acknowledgments: Experimental support by K. Gawlitza, M. Grüneberg and S. Benemann (all BAM) regarding TEM, TGA and SEM measurements, respectively, is gratefully acknowledged.

Conflicts of Interest: The authors declare no conflict of interest.

References

1. Sameiro, M.; Goncalves, T. Fluorescent Labeling of Biomolecules with Organic Probes. *Chem. Rev.* **2009**, *109*, 190–212. [CrossRef]
2. Kramer, J.; Kang, R.; Grimm, L.M.; De Cola, L.; Picchetti, P.; Biedermann, F. Molecular Probes, Chemosensors, and Nanosensors for Optical Detection of Biorelevant Molecules and Ions in Aqueous Media and Biofluids. *Chem. Rev.* **2022**, *122*, 3459–3636. [CrossRef] [PubMed]
3. Resch-Genger, U.; Grabolle, M.; Cavaliere-Jaricot, S.; Nitschke, R.; Nann, T. Quantum dots versus organic dyes as fluorescent labels. *Nat. Methods* **2008**, *5*, 763–775. [CrossRef] [PubMed]
4. Jensen, E.C. Use of fluorescent probes: Their effect on cell biology and limitations. *Anat. Rec.* **2012**, *295*, 2031–2036. [CrossRef] [PubMed]
5. Vogel, R.; Surawski, P.P.T.; Littleton, B.N.; Miller, C.R.; Lawrie, G.A.; Battersby, B.J.; Trau, M. Fluorescent organosilica micro- and nanoparticles with controllable size. *J. Colloid Interface Sci.* **2007**, *310*, 144–150. [CrossRef]
6. Borisov, S.M.; Mayr, T.; Mistlberger, G.; Klimant, I. Dye-Doped Polymeric Particles for Sensing and Imaging. In *Advanced Fluorescence Reporters in Chemistry and Biology II: Molecular Constructions, Polymers and Nanoparticles*; Demchenko, A.P., Ed.; Springer: Heidelberg, Germany, 2010; pp. 193–228. [CrossRef]

7. Gubala, V.; Giovannini, G.; Kunc, F.; Monopoli, M.P.; Moore, C.J. Dye-doped silica nanoparticles: Synthesis, surface chemistry and bioapplications. *Cancer Nanotechnol.* **2020**, *11*, 1. [CrossRef]
8. Visaveliya, N.R.; Köhler, J.M. Softness Meets with Brightness: Dye-Doped Multifunctional Fluorescent Polymer Particles via Microfluidics for Labeling. *Adv. Opt. Mater.* **2021**, *9*, 2002219. [CrossRef]
9. Djoba Siawaya, J.F.; Roberts, T.; Babb, C.; Black, G.; Golakai, H.J.; Stanley, K.; Bapela, N.B.; Hoal, E.; Parida, S.; Van Helden, P. An evaluation of commercial fluorescent bead-based luminex cytokine assays. *PLoS ONE* **2008**, *3*, e2535. [CrossRef]
10. Spiro, A.; Lowe, M.; Brown, D. A bead-based method for multiplexed identification and quantitation of DNA sequences using flow cytometry. *Appl. Environ. Microbiol.* **2000**, *66*, 4258–4265. [CrossRef]
11. Sarma, D.; Gawlitza, K.; Rurack, K. Polystyrene Core–Silica Shell Particles with Defined Nanoarchitectures as a Versatile Platform for Suspension Array Technology. *Langmuir* **2016**, *32*, 3717–3727. [CrossRef]
12. Sarma, D.; Carl, P.; Climent, E.; Schneider, R.J.; Rurack, K. Multifunctional polystyrene core/silica shell microparticles with antifouling properties for bead-based multiplexed and quantitative analysis. *ACS Appl. Mater. Interfaces* **2018**, *11*, 1321–1334. [CrossRef] [PubMed]
13. Hiruta, Y.; Nemoto, R.; Kanazawa, H. Design and synthesis of temperature-responsive polymer/silica hybrid nanoparticles and application to thermally controlled cellular uptake. *Colloids Surfaces B* **2017**, *153*, 2–9. [CrossRef] [PubMed]
14. Tobias, C.; Climent, E.; Gawlitza, K.; Rurack, K. Polystyrene microparticles with convergently grown mesoporous silica shells as a promising tool for multiplexed bioanalytical assays. *ACS Appl. Mater. Interfaces* **2021**, *13*, 207–218. [CrossRef] [PubMed]
15. Schmitt, M.; Bravo, I.; Snijders, P.J.; Gissmann, L.; Pawlita, M.; Waterboer, T. Bead-based multiplex genotyping of human papillomaviruses. *J. Clin. Microbiol.* **2006**, *44*, 504–512. [CrossRef] [PubMed]
16. Loudet, A.; Burgess, K. BODIPY dyes and their derivatives: Syntheses and spectroscopic properties. *Chem. Rev.* **2007**, *107*, 4891–4932. [CrossRef]
17. Liu, J.; Sun, L.; Zhan, H.; Fan, L.-F. Preparation of Fluorescence-Encoded Microspheres Based on Hydrophobic Conjugated Polymer–Dye Combination and the Immunoassay. *ACS Appl. Bio Mater.* **2019**, *2*, 3009–3018. [CrossRef]
18. Elshal, M.F.; McCoy, J.P. Multiplex bead array assays: Performance evaluation and comparison of sensitivity to ELISA. *Methods* **2006**, *38*, 317–323. [CrossRef]
19. Birtwell, S.; Morgan, H. Microparticle encoding technologies for high-throughput multiplexed suspension assays. *Integr. Biol.* **2009**, *1*, 345–362. [CrossRef]
20. Nolan, J.P.; Sklar, L.A. Suspension array technology: Evolution of the flat-array paradigm. *Trends Biotechnol.* **2002**, *20*, 9–12. [CrossRef]
21. Harich, R.; Roger, C.; Garnier, L.; Bienvenu, J.; Fabien, N. Comparison of anti-CCP autoantibodies measurement by ELISA and a bead-based assay in a large patient cohort. *Clin. Biochem.* **2014**, *47*, 485–488. [CrossRef]
22. Fulton, R.J.; McDade, R.L.; Smith, P.L.; Kienker, L.J.; Kettman, J.R. Advanced multiplexed analysis with the FlowMetrixTM system. *Clin. Chem.* **1997**, *43*, 1749–1756. [CrossRef] [PubMed]
23. Dannhardt, G.; Kiefer, W.; Krämer, G.; Maehrlein, S.; Nowe, U.; Fiebich, B. The pyrrole moiety as a template for COX-1/COX-2 inhibitors. *Eur. J. Med. Chem.* **2000**, *35*, 499–510. [CrossRef] [PubMed]
24. Peseke, K.; Götze, L.; Reinke, H.; Cedeño, Q.A.; Suarez, J.Q.; Andreu, M.G.; Castro, H.V. A Synthesis of Substituted Tetrahydro-2-pyranols. *J. Prakt. Chem.* **1997**, *339*, 656–659. [CrossRef]
25. Gresser, R.; Hartmann, H.; Wrackmeyer, M.; Leo, K.; Riede, M. Synthesis of thiophene-substituted aza-BODIPYs and their optical and electrochemical properties. *Tetrahedron* **2011**, *67*, 7148–7155. [CrossRef]
26. Arroyo, I.J.; Hu, R.; Tang, B.Z.; López, F.I.; Peña-Cabrera, E. 8-Alkenylborondipyrromethene dyes. General synthesis, optical properties, and preliminary study of their reactivity. *Tetrahedron* **2011**, *67*, 7244–7250. [CrossRef]
27. Gresser, R.; Hummert, M.; Hartmann, H.; Leo, K.; Riede, M. Synthesis and characterization of near-infrared absorbing benzannulated aza-BODIPY dyes. *Chem. Eur. J.* **2011**, *17*, 2939–2947. [CrossRef] [PubMed]
28. Majumdar, P.; Mack, J.; Nyokong, T. Synthesis, characterization and photophysical properties of an acenaphthalene fused-ring-expanded NIR absorbing aza-BODIPY dye. *RSC Adv.* **2015**, *5*, 78253–78258. [CrossRef]
29. Gorman, A.; Killoran, J.; O'Shea, C.; Kenna, T.; Gallagher, W.M.; O'Shea, D.F. In vitro demonstration of the heavy-atom effect for photodynamic therapy. *J. Am. Chem. Soc.* **2004**, *126*, 10619–10631. [CrossRef]
30. Armbruster, D.A.; Pry, T. Limit of blank, limit of detection and limit of quantitation. *Clin. Biochem. Rev.* **2008**, *29* (Suppl. S1), S49–S52.
31. Soto-Cantu, E.; Cueto, R.; Koch, J.; Russo, P.S. Synthesis and rapid characterization of amine-functionalized silica. *Langmuir* **2012**, *28*, 5562–5569. [CrossRef]
32. Hong, J.; Han, H.; Hong, C.K.; Shim, S.E. A direct preparation of silica shell on polystyrene microspheres prepared by dispersion polymerization with polyvinylpyrrolidone. *J. Polym. Sci. A* **2008**, *46*, 2884–2890. [CrossRef]
33. Sarma, D.; Mielke, J.; Sahre, M.; Beck, U.; Hodoroaba, V.-D.; Rurack, K. TSEM-based contour analysis as a tool for the quantification of the profile roughness of silica shells on polystyrene core particles. *Appl. Surf. Sci.* **2017**, *426*, 446–455. [CrossRef]
34. Lu, H.; Mack, J.; Yang, Y.; Shen, Z. Structural modification strategies for the rational design of Red/NIR region BODIPYs. *Chem. Soc. Rev.* **2014**, *43*, 4778–4823. [CrossRef] [PubMed]
35. Lagorio, M.G.; Román, E.S. How does light scattering affect luminescence? Fluorescence spectra and quantum yields in the solid phase. *J. Chem. Educ.* **2002**, *79*, 1362–1367. [CrossRef]

36. Castillo-Hair, S.M.; Sexton, J.T.; Landry, B.P.; Olson, E.J.; Igoshin, O.A.; Tabor, J.J. FlowCal: A User-Friendly, Open Source Software Tool for Automatically Converting Flow Cytometry Data from Arbitrary to Calibrated Units. *ACS Synth. Biol.* **2016**, *5*, 774–780. [CrossRef] [PubMed]
37. Friedman, M.; Williams, L.D. Stoichiometry of formation of Ruhemann's purple in the ninhydrin reaction. *Bioorg. Chem.* **1974**, *3*, 267–280. [CrossRef]
38. Leng, W.; Chen, M.; Zhou, S.; Wu, L. Capillary force induced formation of monodisperse polystyrene/silica organic− inorganic hybrid hollow spheres. *Langmuir* **2010**, *26*, 14271–14275. [CrossRef]
39. Schneider, C.A.; Rasband, W.S.; Eliceiri, K.W. NIH Image to ImageJ: 25 years of image analysis. *Nat. Methods* **2012**, *9*, 671–675. [CrossRef]
40. Corrie, S.R.; Lawrie, G.A.; Trau, M. Quantitative analysis and characterization of biofunctionalized fluorescent silica particles. *Langmuir* **2006**, *22*, 2731–2737. [CrossRef]
41. Song, X.; Gao, L. Fabrication of hollow hybrid microspheres coated with silica/titania via sol− gel process and enhanced photocatalytic activities. *J. Phys. Chem. C* **2007**, *111*, 8180–8187. [CrossRef]
42. Rollié, S.; Sundmacher, K. Determination of cluster composition in heteroaggregation of binary particle systems by flow cytometry. *Langmuir* **2008**, *24*, 13348–13358. [CrossRef] [PubMed]
43. Descalzo, A.B.; Xu, H.-J.; Xue, Z.-L.; Hoffmann, K.; Shen, Z.; Weller, M.G.; You, X.-Z.; Rurack, K. Phenanthrene-fused boron− dipyrromethenes as bright long-wavelength fluorophores. *Org. Lett.* **2008**, *10*, 1581–1584. [CrossRef] [PubMed]
44. Behnke, T.; Würth, C.; Hoffmann, K.; Hübner, M.; Panne, U.; Resch-Genger, U. Encapsulation of hydrophobic dyes in polystyrene micro-and nanoparticles via swelling procedures. *J. Fluoresc.* **2011**, *21*, 937–944. [CrossRef]
45. Wittmershaus, B.P.; Baseler, T.T.; Beaumont, G.T.; Zhang, Y.-Z. Excitation energy transfer from polystyrene to dye in 40-nm diameter microspheres. *J. Lumin.* **2002**, *96*, 107–118. [CrossRef]
46. Horejsh, D.; Martini, F.; Poccia, F.; Ippolito, G.; Di Caro, A.; Capobianchi, M.R. A molecular beacon, bead-based assay for the detection of nucleic acids by flow cytometry. *Nucleic Acids Res.* **2005**, *33*, e13. [CrossRef] [PubMed]
47. Thiollet, S.; Higson, S.; White, N.; Morgan, S.L. Investigation and development of quantum dot-encoded microsphere bioconjugates for DNA detection by flow cytometry. *J. Fluoresc.* **2012**, *22*, 685–697. [CrossRef] [PubMed]
48. AbCam ELISA Kits Specifications. Available online: http://www.abcam.com (accessed on 30 October 2022).
49. Momenbeitollahi, N.; Cloet, T.; Li, H. Pushing the detection limits: Strategies towards highly sensitive optical-based protein detection. *Anal. Bioanal. Chem.* **2021**, *413*, 5995–6011. [CrossRef] [PubMed]
50. Selvarajah, S.; Negm, O.H.; Hamed, M.R.; Tubby, C.; Todd, I.; Tighe, P.J.; Harrison, T.; Fairclough, L.C. Development and validation of protein microarray technology for simultaneous inflammatory mediator detection in human sera. *Mediators Inflamm.* **2014**, *2014*, 820304. [CrossRef]
51. Haab, B.B.; Dunham, M.J.; Brown, P.O. Protein microarrays for highly parallel detection and quantitation of specific proteins and antibodies in complex solutions. *Genome Biol.* **2001**, *2*, research0004.1. [CrossRef]